Journal of Crystal Growth 311 (2009) 3239–3242

Contents lists available at ScienceDirect

Journal of Crystal Growth

journal homepage: www.elsevier.com/locate/jcrysgro

Defect reduction in nonpolar and semipolar GaN using scandium nitride interlayers

M.A. Moram *, C.F. Johnston, M.J. Kappers, C.J. Humphreys

Department Materials Science & Metallurgy, University of Cambridge, Pembroke Street, Cambridge CB2 3QZ, UK

ARTICLE INFO

Article history:
Received 28 February 2009
Accepted 23 March 2009
Communicated by M. Schieber
Available online 1 April 2009

PACS:
61.05.cp
61.72.Dd
61.72.Lk
61.72.Nn
81.05.Ea
81.15.Gh

Keywords:
A1. Crystal structure
A1. Line defects
A1. Planar defects
A3. Metalorganic vapour phase epitaxy
B1. Nitrides
B2. Semiconducting III–V materials

ABSTRACT

Nonpolar $(11\bar{2}0)$ and semipolar $(11\bar{2}2)$ GaN films were grown on sapphire by metalorganic vapour phase epitaxy using ScN interlayers of varying thicknesses. A 5 nm interlayer reduced basal plane stacking fault (BSF) densities in nonpolar films by a factor of 2 and threading dislocation (TD) densities by a factor of 100 to $(1.8 \pm 0.2) \times 10^9\,cm^{-2}$. An 8.5 nm interlayer reduced BSF densities in semipolar films by a factor of 5 and reduced TD densities by a factor of 200 to $(1.5 \pm 0.3) \times 10^8\,cm^{-2}$. Nonpolar film surface roughnesses were reduced by a factor of 20.

1. Introduction

A III-nitride light-emitting devices are conventionally based on 'polar' [0 0 0 1]-oriented GaN films. Since the wurtzite structure lacks a centre of symmetry, a piezoelectric and spontaneous polarization exist along [0 0 0 1], resulting in an internal electric field in this direction (i.e. perpendicular to the device quantum well regions). This causes the band structure to bend, reducing the overlap of the electron and hole wavefunctions in the quantum wells of the device resulting in longer radiative lifetimes and lower device efficiencies [1]. The effects of the internal electric field need to be reduced or eliminated in order to increase light emission efficiencies. One method is by using devices based on nonpolar *m*-plane $(10\bar{1}0)$ or *a*-plane $(11\bar{2}0)$ films, in which the internal electric field lies in the plane of the film, preventing band bending across the quantum wells [2]. The semipolar $(10\bar{1}1)$ or $(11\bar{2}2)$ orientations can also be used, allowing only a reduced component of the electric field to be directed across the quantum wells. However, both nonpolar and semipolar heteroepitaxial films typically contain very high densities of defects compared to the best polar *c*-plane films. Nonpolar films grown without defect-reduction techniques usually contain basal plane stacking faults (BSFs) oriented perpendicular to the film surface (densities as high as $10^6\,cm^{-1}$) together with partial dislocations bounding the BSFs and pure threading dislocations (TD) (combined densities as high as $10^{11}\,cm^{-2}$) [3,4]. Semipolar films contain similar types and densities of defects, but in these orientations the BSFs and their associated partial dislocations are inclined with respect to the film surface [5]. Defect-reduction techniques (such as the use of SiN_x interlayers [6–8], epitaxial lateral overgrowth (ELOG) [9] and island growth mode control [10]) that were developed for *c*-plane films have been applied to nonpolar and semipolar films [11–15]. Some defect reduction is typically observed, but there are often key differences compared to the results obtained for polar films, due to the very different film microstructures and growth modes. The use of ScN interlayers has recently been shown to reduce defect densities in *c*-plane material substantially [16,17]. In this study, we show that ScN interlayers are particularly effective for

*Corresponding author.
E-mail address: mam65@cam.ac.uk (M.A. Moram).

0022-0248/$ - see front matter © 2009 Elsevier B.V. All rights reserved.
doi:10.1016/j.jcrysgro.2009.03.029

defect reduction in nonpolar and semipolar films and we compare the defect-reduction mechanism with that postulated for *c*-plane films.

2. Experimental details

A series of nonpolar $(11\bar{2}0)$ and semipolar $(11\bar{2}2)$ GaN films were grown by metalorganic vapour phase epitaxy (MOVPE) in a Thomas Swan $6\times2''$ close-coupled showerhead reactor. The nonpolar *a*-plane $(11\bar{2}0)$ films were grown on *r*-plane $(1\bar{1}02)$ sapphire, whereas the semipolar $(11\bar{2}2)$ films were grown on *m*-plane $(10\bar{1}0)$ sapphire. A set of nonpolar template films were grown at a low V/III ratio of 200 to promote lateral growth and smooth films; growth details are given in Ref. [18]. A set of semipolar template films were grown using an initial islanded growth mode (a V/III ratio of 715 for 300 s), followed by island coalescence at a higher V/III ratio of 1075. Subsequently, both types of template films were removed from the reactor and Sc metal layers of thicknesses varying from 2 to 15 nm were deposited externally using magnetron sputtering. The coated templates were then subjected to a nitridation/annealing step in the growth reactor to produce ScN (Sc deposition and annealing conditions were similar to those given in Ref. [16]). For nonpolar films, subsequent epilayer growth was performed using 7200 s GaN growth at 1020 °C and 100 Torr with a TMG flow of 340 μmol min^{-1} and an NH_3 flow of 67 μmol min^{-1}. For semipolar films, subsequent GaN overgrowth was performed using 600 s GaN growth at 1020 °C and 100 Torr with a trimethylgallium (TMG) flow of 426 μmol min^{-1} and an NH_3 flow of 446 μmol min^{-1}, followed by 5700 s growth at a reduced NH_3 flow of 84 μmol min^{-1}. Epilayers of both orientations were grown to a thickness of approximately 5.2 μm. Transmission electron microscopy (TEM) analysis was performed using a Philips CM30 microscope operated at 300 kV. Both cross-sectional and plan-view TEM samples were prepared by mechanical polishing and ion beam milling to electron transparency. Threading dislocation densities were obtained from plan-view images using g=0002 (in which partial dislocations (b=1/6$\langle 20\bar{2}3\rangle$), pure *a*+*c*-type TDs (b=1/3$\langle 11\bar{2}3\rangle$) and pure *c*-type TDs (b=[0 0 0 1]) are visible) and g=1$\bar{1}$02 (in which *a*-type TDs show residual contrast). The density and average length of BSFs (R=1/6$\langle 20\bar{2}3\rangle$) were found using g=1$\bar{1}$00 and calculated from the total length of stacking faults per unit area [15]. X-ray diffraction (XRD) was performed with CuKα_1 radiation of wavelength 1.54059 Å [19] using a P'Analytical X-Pert Pro MRD diffractometer with a mirror, a four-bounce asymmetric Ge (2 2 0) monochromator and a triple-bounce analyser. Atomic force microscopy (AFM) was performed using a Digital Instruments Nanoscope Dimension 3100 microscope and the data analysed using the WsXM software [20].

3. Results and discussion

XRD ω-scans were initially used to identify trends in defect densities throughout the series of samples with varying interlayer thicknesses. TEM studies on similar samples [21] indicated that the final ScN interlayer thickness did not differ strongly from the thickness of the original Sc layer. Fig. 1 shows the full-width at half-maximum (FWHM) of ω-scans of the symmetric 11$\bar{2}$0 reflection of the nonpolar *a*-plane films, used as an approximate guide to the film structural quality (note that films grown using interlayer thicknesses greater than 8.5 nm did not coalesce, so the FWHM data were not used as the comparison was not valid). As the FWHM varies with the in-plane rotational orientation of the sample, the FWHM was recorded with the sample oriented in-plane both parallel and perpendicular to [0 0 0 1] (the directions in which the FWHM showed a maximum or minimum). These data suggested that an interlayer thickness of 5 nm was optimum, as that sample showed both the lowest overall ω-FWHM values and the lowest ω-FWHM anisotropy with respect to the sample's in-plane rotational orientation. However, because the 11$\bar{2}$0 reflection is not affected by I_1 or I_2 BSFs (the types most likely to be present [3,4]), the 11$\bar{2}$0 XRD data are sensitive only to partial dislocation densities and to other factors such as mosaic tilt or twist [19] (wafer curvature did not differ significantly between samples and was thus ignored when interpreting XRD ω-scan trends). Therefore, skew symmetric ω-scans of the $h0\bar{h}0$ series of reflections (of which 10$\bar{1}$0 and 20$\bar{2}$0 are affected by BSFs but 30$\bar{3}$0 is not) were also obtained for each sample, but no clear data trends that could be attributed to changes in BSF density were apparent. These data suggest that BSF densities did not vary strongly throughout the sample series, but that partial dislocation densities and mosaic tilt varied more significantly. For these nonpolar films, AFM data showed that the insertion of ScN interlayers was also accompanied by a reduction of the r.m.s. surface roughness by approximately a factor of 20, when compared to a control sample grown to the same thickness but without any interlayer (Fig. 2). In particular, the surface pits observed in the control sample disappeared upon introduction of the interlayer.

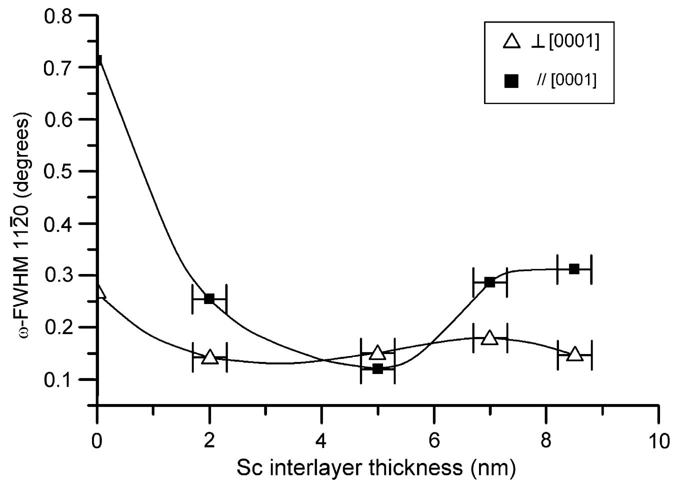

Fig. 1. Variation of the full-width at half-maximum (FWHM) of the symmetric 11$\bar{2}$0 ω-scan peak at two different in-plane rotational orientations (inset) versus the thickness of the Sc interlayer as originally deposited.

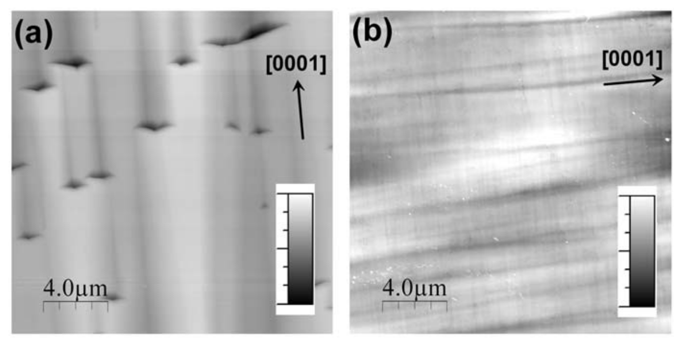

Fig. 2. A 20 μm × 20 μm atomic force microscopy images of: (a) a nonpolar film without a ScN interlayer (height scale: 900 nm, r.m.s. roughness of 73 nm) and (b) a nonpolar film grown under similar conditions using a 5 nm ScN interlayer (height scale: 40 nm, r.m.s. roughness 4 nm). The in-plane [0 0 0 1] direction is indicated on each image.